Mon. Not. R. Astron. Soc. **312**, 103–115 (2000)

# Polarimetry of young stellar objects – III. Circular polarimetry of OMC-1

Antonio Chrysostomou,[1,2★] T. M. Gledhill,[1] François Ménard,[3,4] J. H. Hough,[1] Motohide Tamura[5] and Jeremy Bailey[6]

[1]*Department of Physical Sciences, University of Hertfordshire, Hatfield AL10 9AB*
[2]*Joint Astronomy Centre, 660 N. A'ohōkū Place, Hilo, HI 96720, USA*
[3]*Laboratoire d'Astrophysique de l'Observatoire de Grenoble, CNRS/UJF UMR 5571, BP-53, 38041 Grenoble Cedex, France*
[4]*Canada–France–Hawaii Telescope Corporation, PO Box 1597, Kamuela, HI 96743, USA*
[5]*National Astronomical Observatory, Osawa 2-21-1, Mitaka, Tokyo 181, Japan*
[6]*Anglo-Australian Observatory, Epping, NSW 2121, Australia*

Accepted 1999 September 3. Received 1999 August 20; in original form 1999 May 28



**ABSTRACT**

We present the first imaging circular polarimetry of the Orion Molecular Cloud, OMC-1. The observations, taken in the $J$, $H$, $K_n$ and nb$L$ bands, reveal a complex pattern of circular polarization. Globally, there is a background circular polarization of the order of $\pm 2$ per cent in the $K_n$ band, conforming to the typical quadrupolar patterns that have been observed in other outflow sources. Overlying this pattern are regions of relatively high degrees of circular polarization to the east and west of the source IRc2, with degrees as high as $+17$ per cent in the $K_n$ band, the highest circular polarization yet measured for any young stellar object. No circular polarization is seen in the $J$ band, indicating that the circular polarization detected at longer wavelengths originates from within OMC-1 and not from scattering off the foreground ionization front associated with the M42 nebula.

We demonstrate a correlation between these patches of high circular polarization and regions of enhanced linear polarization, and argue that these observations are best explained using a model that incorporates scattering of radiation off oblate grains, which have been aligned by the local magnetic field. Modelling of the ellipticity (the ratio of circular to linear polarization) suggests that the grains are composed of silicate and/or organic refractory material, and that grains larger than are typically found in the interstellar medium are needed. The lower, background, circular polarization is produced by scattering off randomly oriented grains in the outflow cavities, the grain alignment being destroyed by the passage of shocks.

We put forward a morphological model for OMC-1 which has the regions of high polarization separate from, but near to, the main outflow region. Those regions exhibiting high polarization must somehow have a direct view of the illuminating source of the nebula.

Implications of this work to the origins of life are briefly discussed.

**Key words:** polarization – scattering – stars: pre-main-sequence – ISM: individual: OMC-1 – ISM: jets and outflows – reflection nebulae.

## 1 INTRODUCTION

The Orion Molecular Cloud, OMC-1, has been studied using the technique of polarimetry quite extensively at most wavelengths (Gonatas et al. 1990; Minchin et al. 1991; Aitken et al. 1997, for example). In the main, these studies have confined themselves to linear polarimetry with hardly any circular polarimetry conducted at all. Those observations attempted were aperture-based and towards either point sources or field stars (Lonsdale et al. 1980). In these studies, the circular polarization was interpreted in terms of radiation passing through a medium of aligned grains where the alignment direction is not constant.

It is also possible to produce circular polarization by scattering mechanisms. Single scattering of unpolarized light off spherical grains will not produce any circular polarization. However, if that same scattering occurs for polarized radiation it is possible to induce significant amounts of circular polarization, depending on the grain material (chiefly, the absorptive component of the refractive index), scattering angles and incident linear polarization.

★ E-mail: a.chrysostomou@star.herts.ac.uk

As a rule of thumb, the degrees of linear and circular polarization work in opposing senses for scattering off spherical grains: i.e. small grains produce high degrees of linear polarization and only very small degrees of circular polarization, and vice versa. Indeed, at the Rayleigh limit for small grains, it is not possible to produce any circular polarization, while the linear polarization can be at its maximum of 100 per cent for a 90° scatter (Shafter & Jura 1980).

Clearly, measurement of circular polarization is important in the study of stellar environments, especially where outflow phenomena are present, as it makes it possible to probe the morphology and structure of the inner and highly obscured central regions, where photons are initially polarized, as well as the composition of the grains which form part of the basic material of the accreting matter.

The measurement of circular polarization is inherently difficult in regions where linear polarization is high, such as in reflection nebulae, owing to the difficulty of separating the linearly and circularly polarized components of the radiation. Recently we have been able to overcome this difficulty, to obtain the first images of circular polarization from extended sources (Gledhill, Chrysostomou & Hough 1996; Chrysostomou et al. 1997a). These observations, of the low-mass pre-main-sequence sources Chamaeleon Infrared Nebula and GSS 30, provided the discovery of significant degrees of circular polarization in bipolar reflection nebulae. The interpretation of these results required photons to be rapidly polarized near the source before escaping into the outflow cavity, thus invoking the need for a dusty envelope close to the inner source.

The data presented in this paper represent the first imaging circular polarimetry of OMC-1, a high-mass star-forming region. The results obtained show a stark contrast to the low-mass sources, with degrees of circular polarization an order of magnitude greater. In the following sections, we describe how the circular polarimetry data were obtained, then present the results and compare them with other complementary data sets. Most existing models have thus far only considered scattering from spherical grains. Here, we apply a model that calculates scattering off aligned aspherical grains (Gledhill & McCall, in preparation) to analyse our results. Finally, we discuss the implications of these results for the cloud morphology and briefly comment on their significance to the origins of life.

## 2 OBSERVATIONS

### 2.1 AAT observations

Circular polarimetric observations of OMC-1, in the $J$, $H$ and $K_n$ bands, were obtained on the night of 1996 November 20 at the 3.9-m Anglo-Australian Telescope (AAT), Siding Spring, Australia. The facility infrared imager–spectrometer, IRIS, was used at the *f*/15 telescope focus using instrument optics that provided a 0.6-arcsec pixel scale.

Polarimetry with IRIS is obtained with the infrared polarimetry module IRISPOL, built and designed by the University of Hertfordshire, placed upstream of IRIS while a cold $MgF_2$ Wollaston prism within the instrument splits the incoming radiation into the orthogonally polarized extraordinary (e-) and ordinary (o-) beams. This acts as the polarimetric analyser. A focal plane mask within the cryostat masks off half of the field to enable the e- and o-beams to be projected on to the array with minimum overlap. This effectively reduces the field of view to two strips of $\sim 75 \times 20$ arcsec$^2$, separated by $\sim 20$ arcsec.

The OMC-1 data were centred on the Becklin–Neugebauer (BN) object [$\alpha = 5^h\,35^m\,14\overset{s}{.}12$, $\delta = -5°\,22'\,22\overset{''}{.}9$, J2000: Menten & Reid (1995)], using a four-point east–west jitter pattern at each field position. A map of the region was obtained by offsetting the telescope by 15 arcsec in declination from each field position.

Exposure times were 2 s with 30 co-adds per waveplate position in the $K_n$ and $H$ bands, and 6 s with 10 co-adds in the $J$ band. The $K_n$ filter is optimized to reduce the thermal background at the long-wavelength end, and the effect of water vapour at the short-wavelength end of the filter passband (2.0–2.3 μm). The BN object was saturated in the $K_n$ filter.

### 2.2 UKIRT observations

Circular polarimetric observations of OMC-1 through a 1 per cent filter at 3.6 μm (the nb$L$ filter) were obtained on the night of 1998 January 29 at the 3.8-m United Kingdom Infrared Telescope (UKIRT) on the summit of Mauna Kea, Hawaii. The facility infrared camera, IRCAM3, was used at the *f*/36 Cassegrain focus. The pixel scale of the camera was 0.28 arcsec per pixel.

The polarimetry module of UKIRT, IRPOL2 (similarly designed and built at the University of Hertfordshire), operates in an almost identical manner to IRISPOL at the AAT. Inside IRCAM3 there is a cold lithium niobate ($LiNbO_4$) Wollaston prism. The focal plane mask is exterior to the dewar, i.e. it is warm. The field of view through each aperture of the mask is similar to that of IRISPOL.

Observations of OMC-1 were secured by performing a three-point east–west jitter pattern at each position of the telescope and waveplate. The field was mapped by observing at four positions, each separated by 10 arcsec in declination. The integration time was constructed from 100 co-adds of 0.15-s exposure.

### 2.3 Circular polarimetry: data acquisition and reduction

Light is, in general, elliptically polarized, and any transmission of the linear component by the instrument can be spuriously measured as circular polarization. This problem is counteracted by continuously rotating a λ/2 retarder above a stepped λ/4 retarder. This effectively cancels the linear component over a single integration, given that (i) the exposure time is an integer multiple of the λ/2 retarder rotation period, and (ii) the λ/2 retarder rotation period is small with respect to the total integration time. The rejection factor of the linearly polarized component is as high as 2000.

Circular polarimetry requires observations at two angular positions of the achromatic λ/4 retarder, separated by 90° and set to give the maximum modulation of the $V$ Stokes parameter. This is how observations were collected with IRISPOL at the AAT.

An alternative method for measuring circular polarization can be used when the angular positions of maximum modulation of the $V$ vector are not known for the retarder. This involves rotating the λ/4 retarder to four set positions: 0°, 90°, 45° and 135°. This method was employed at UKIRT for what was then a new $L$-band, zero-order λ/4 retarder.

The efficiency for measuring circular polarization with both instruments is estimated to be at least 95 per cent and perhaps higher (Chrysostomou et al. 1997a, for further details).

Stokes parameters can be calculated by use of the following

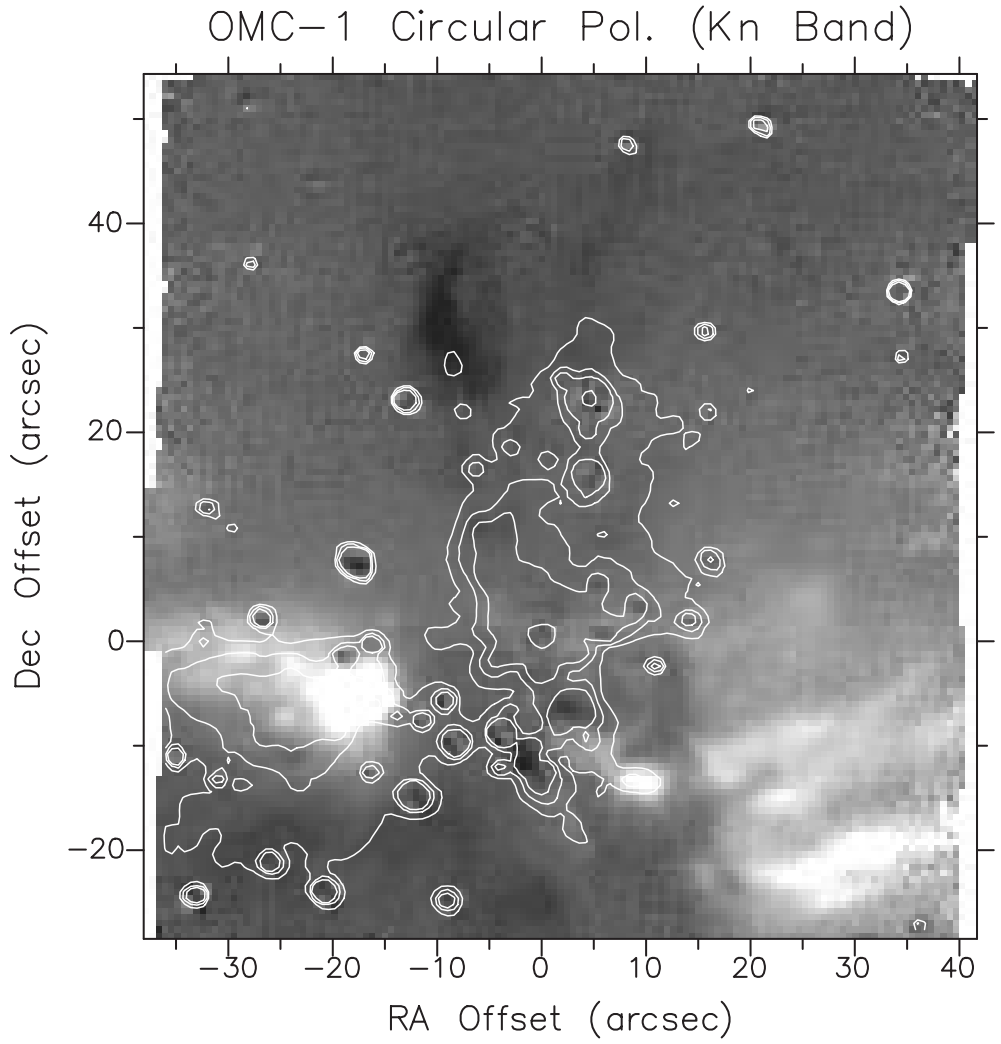


**Figure 1.** $K_n$-band circular polarization image of the core region of OMC-1. The circular polarization is scaled between −5 per cent (black) and +10 per cent (white). Overlaid are surface brightness contours outlining the positions of field stars and the diffuse emission. Offsets are west relative to the BN object.

expression:

$$\frac{\left[\frac{(e/o)_\alpha}{(e/o)_\beta}\right]^{0.5}-1}{\left[\frac{(e/o)_\alpha}{(e/o)_\beta}\right]^{0.5}+1}, \qquad (1)$$

where $e$ and $o$ refer to the intensities of the e- and o-beams at the two retarder positions $\alpha$ and $\beta$. For the data obtained at the AAT, the two angular positions observed and equation (1) give the intensity-normalized $V$ Stokes parameter directly.

In general, when four angular positions are measured, the $V$ Stokes parameter is determined by adding in quadrature the result from equation (1) for observations at 0° and 90° with those for 45° and 135°. In the final analysis of the UKIRT nb$L$-band data, it was determined that most, if not all, of the circular polarization was modulating between the 45° and 135° positions, with the Stokes parameter calculated from the 0° and 90° positions having no modulated polarization signal. Thus all circular polarization measurements quoted and presented for the nb$L$ band in this paper are derived from the 45° and 135° positions only.[1]

Standard data reduction techniques were employed to produce flat-fielded and sky-subtracted images, the flat-fields constructed from a median filter of sky images obtained during the night.

## 3 RESULTS

### 3.1 The data

In Fig. 1, $K_n$-band imaging circular polarimetry of OMC-1 is presented, overlaid with intensity contours – the lowest contour approximately delineates the outflow cavity which is better traced by the $H_2$ emission (Allen & Burton 1993, for example). The circular polarization is plotted between −5 and +10 per cent, where the ± signs correspond to left- and right-handed circular

[1] Subsequent to these observations, the angles for maximum modulation of the $V$ Stokes parameter were determined to be 38° and 128°. This 7° difference results in a reduced efficiency of 4 per cent which is not significant for our results.

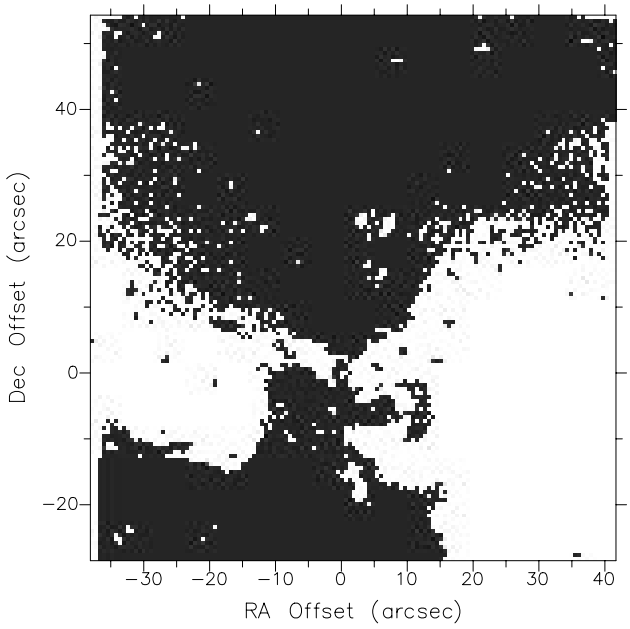


**Figure 2.** $K_n$-band circular polarimetry image from Fig. 1 after it has been thresholded to display all values with $V/I < 0$ as black and all values with $V/I > 0$ as white. This representation clearly shows the 'quadrupolar' structure of the background circular polarization in the OMC-1 region.

polarization, respectively, as viewed by the observer (i.e. clockwise and anti-clockwise).

The circular polarization is quite extensive across the OMC-1 region. Areas of negative circular polarization exist to the north and south of the region, while to the east and west there are large areas of positive circular polarization. Together, these regions form the typical 'quadrupolar' pattern recently observed in low-mass outflow sources (Gledhill et al. 1996; Chrysostomou et al. 1997a), and predicted by Monte Carlo scattering models (Fischer, Henning & Yorke 1996). This pattern is made clear in Fig. 2, which shows Fig. 1 plotted so that white regions represent areas with positive circular polarization while black regions denote negative circular polarization. This pattern naturally arises owing to the rotation of the scattering plane with respect to a central polarized source (Shafter & Jura 1980).

Together with this general pattern are regions of high circular polarization. To the south-east of BN the degree of circular polarization peaks at +17 per cent, in a region that is coincident with strong reflection nebulosity (Werner, Capps & Dinnerstein 1983; Minchin et al. 1991) which is highly linearly polarized (Minchin et al. 1991, ~40 per cent in the $K$ band). This region, first referred to as SEBN by Aitken et al. (1985), corresponds to the highest degrees of circular polarization in OMC-1, or for any young stellar object yet observed.

There is a more widespread area to the south-west of OMC-1 for which the peak polarization is of the order of +12 per cent. Also, at approximately 10 arcsec east and 30 arcsec north of BN is a relatively small region polarized at approximately −5 per cent. A small 'finger' of emission at 10 arcsec west and 13 arcsec south of BN is also quite distinct in the image. This feature does not appear in 10-μm maps (Aitken et al. 1997; Gezari, Backman & Werner 1998) and is not associated with any $H_2$ emission from the OMC-1 outflow (Chrysostomou et al. 1997b; Stolovy et al. 1998), but it is a region of relatively strong polarization (Minchin et al. 1991, and this work).

In Fig. 3, the corresponding $H$-band image is presented with overlying intensity contours. The circular polarization is plotted between −2 and +5 per cent. The same basic features that are present in the $K_n$ band are also present in the $H$ band, including the regions of high circular polarization, although they are not as highly polarized.

Fig. 4 shows a $J$-band image of only a small portion of the region, centred 8 arcsec south of BN, running east–west across SEBN. No circular polarization is detected here at this waveband. This conforms with the conclusions of Minchin et al. (1991) who showed, from their imaging linear polarimetry of OMC-1, that the radiation in the $J$ band originates from the foreground H II region only, the extinction being too great to view the OMC-1 region at this wavelength. Importantly, this lends weight to our assertion that the circular polarization detected in the $H$ and $K_n$ bands do not originate from the foreground H II region, but is intrinsic to the OMC-1 region, although some foreground contamination owing to unpolarized light from the H II region cannot be ruled out.

We have constructed several software apertures across different parts of our data, and measured the $H–K_n$ wavelength dependence as well as the mean and maximum $H$ and $K_n$ circular polarizations within those apertures. The positions of the apertures are shown in Fig. 5 and the results given in Table 1.

There is a clear wavelength dependence in the degrees of circular polarization, the $H$-band polarization being in general 2–3 times lower than that in the $K_n$ band. The near-uniformity of this wavelength dependence suggests that the grain material must also be uniform in composition across the nebula. Sector D, corresponding to the 'finger' of polarization referred to above, seems to present an anomaly to this trend with a much steeper wavelength dependence. Its linear polarimetry indicates that it is definitely associated with the OMC-1 cloud, being illuminated by IRc2. However, the steep wavelength dependence of circular polarization suggests that it is an isolated region the grain properties of which may differ from the rest of the cloud. Examination of the polarization data of Minchin et al. (1991) shows that linear polarization is also lower at this position in the $H$ band. Thus it is more likely that this steeper wavelength dependence is due to extinction effects.

Fig. 6 shows results of the nb$L$ circular polarimetry obtained at UKIRT. The scattered flux in the thermal regime rapidly decreases with distance from the OMC-1 core, necessarily minimizing the extent of the nb$L$-band map. It was thus not possible to search for circular polarization as far north as the region of negative circular polarization which is seen in the $H$ and $K_n$ bands, and low signal-to-noise ratio prevented the detection of any circular polarization in the region approximately 20 arcsec south-west of BN, which is extensively polarized at shorter wavelengths.

The top panel of Fig. 6 gives the circular polarization in the mapped region, while the bottom panel gives the corresponding intensity distribution. Regions of low intensity, and thus low signal-to-noise ratio, have been masked from the circular polarization image. The background 'quadrupolar' pattern of circular polarization has disappeared into the noise. The only feature that clearly remains is the patch of high circular polarization associated with SEBN, with an average circular polarization of the order of +9 per cent. Circular polarization has also been detected towards the small 'finger' region located at (10 arcsec west, 15 arcsec south) from BN (sector D in Fig. 5).

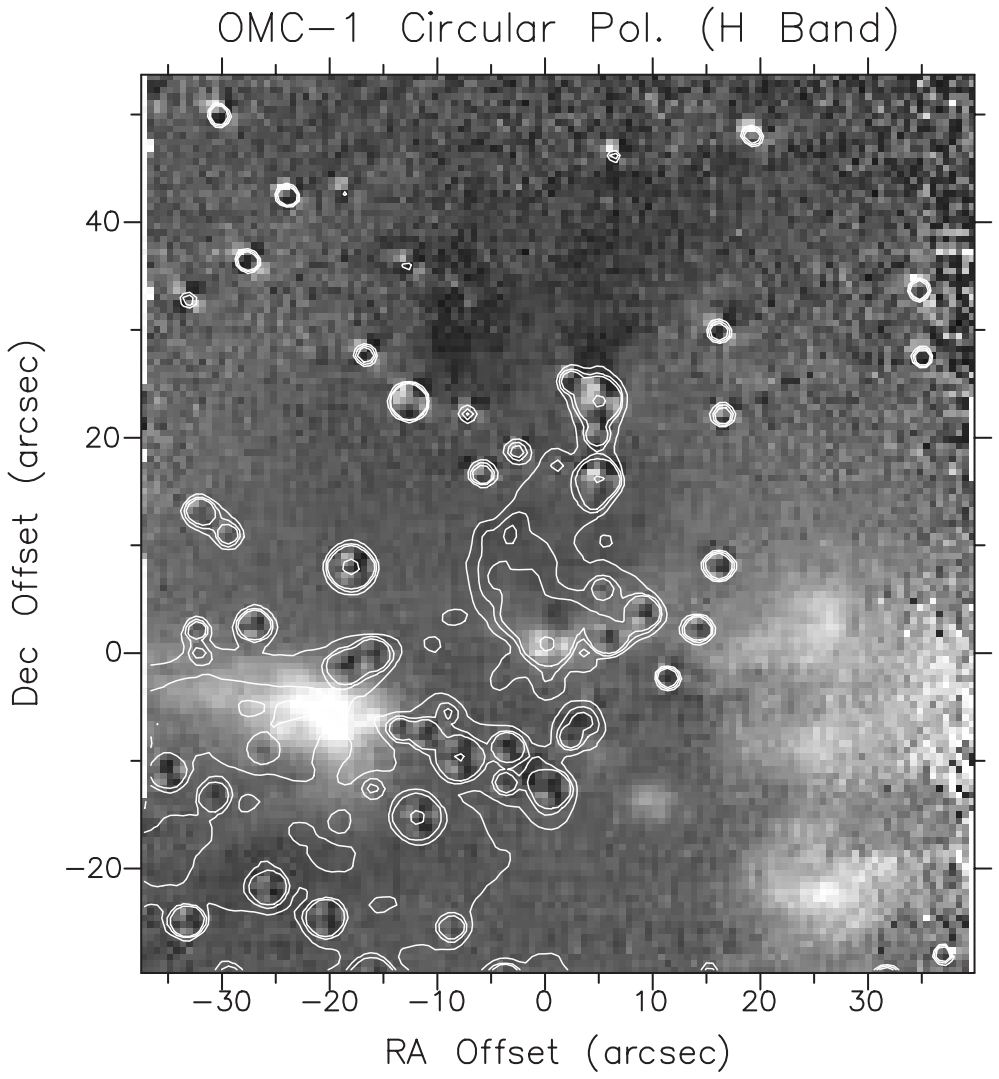


**Figure 3.** As Fig. 1, but for the *H* band. The circular polarization is scaled between −2 per cent (black) and +5 per cent (white). Offsets are west relative to the BN object.

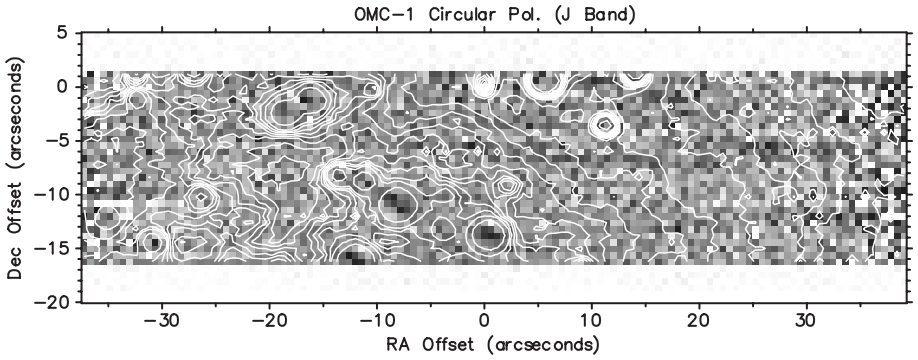


**Figure 4.** *J*-band circular polarization image of a small east–west strip in OMC-1 which stretches across the regions of high circular polarization that are seen in the other infrared bands. The circular polarization is scaled between −2 per cent (black) and +2 per cent (white). Offsets are west relative to the BN object.

### 3.2 Comparison with other data

Fig. 7 compares $K_n$-band circular polarimetry presented here with a recent linear polarimetry image of OMC-1, taken with the 1.3-m ISAS telescope in Japan (Geng 1993). The ISAS data have been re-binned and re-scaled to match our data from the AAT exactly. What is immediately clear is that there is a distinct correlation between regions of high circular and linear polarizations. The spatial extents of these regions are also closely matched.

It is interesting to note that the well-known 'red ridge', which is a highly linearly polarized north-east extension associated with BN (Minchin et al. 1991), finds no counterpart feature in circular

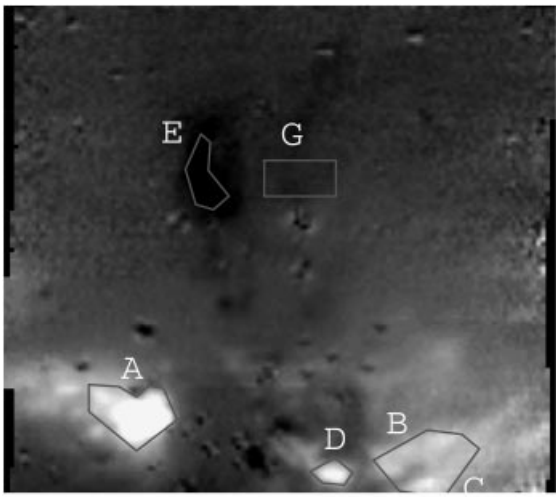


**Figure 5.** $K_n$-band circular polarization image with sectors A–G, used as software apertures in Table 1, outlined.

**Table 1.** Circular polarimetry measurements in OMC-1. Sectors A-G are indicated in Fig. 5.

| | | $H$ | $K_n$ | $K_n/H$ |
|---|---|---|---|---|
| A[a] | Mean | 3.4 | 10.0 | 2.9 |
| | Maximum | 7.4 | 16.6 | 2.2 |
| B | Mean | 1.7 | 6.7 | 3.9 |
| | Maximum | 3.6 | 10.0 | 2.8 |
| C | Mean | 2.6 | 8.9 | 3.4 |
| | Maximum | 5.2 | 13.6 | 2.6 |
| D | Mean | 1.0 | 7.2 | 7.2 |
| | Maximum | 2.1 | 10.5 | 5.0 |
| E | Mean | −1.5 | −4.6 | 3.0 |
| | Maximum | −2.5 | −6.2 | 2.5 |
| F | Mean | −0.5 | −2.1 | 4.2 |
| | Maximum | −1.0 | −2.7 | 2.7 |
| G | Mean | −1.0 | −1.7 | 1.7 |
| | Maximum | −1.8 | −2.2 | 1.2 |

[a] Designated as SEBN in Aitken et al. (1985).

polarimetry.[2] This may indicate that the circular polarization that is measured is dominated by scattering processes within the OMC-1 region and not associated with the BN object, implying either that the natures of the grains differ in the two environments, or that the polarizing mechanisms differ – for example, single scattering of unpolarized light producing relatively high linear polarization with no corresponding circular polarization. Alternatively, the quadrupolar pattern of circular polarization suggests that there are position angles for which no circular polarization can be produced (whereas linear polarization is present for every angle), and the 'red ridge' could be at such an angle relative to its source of illumination.

BN itself is polarized, that polarization arising from the dichroic absorption of radiation by a medium of aligned grains in the line of sight (Aitken et al. 1985; Hough et al. 1996). Lonsdale et al. (1980) measured the circular polarization of

[2] This fact further demonstrates that the high circular polarization that *is* measured is not contamination from high linear polarization.

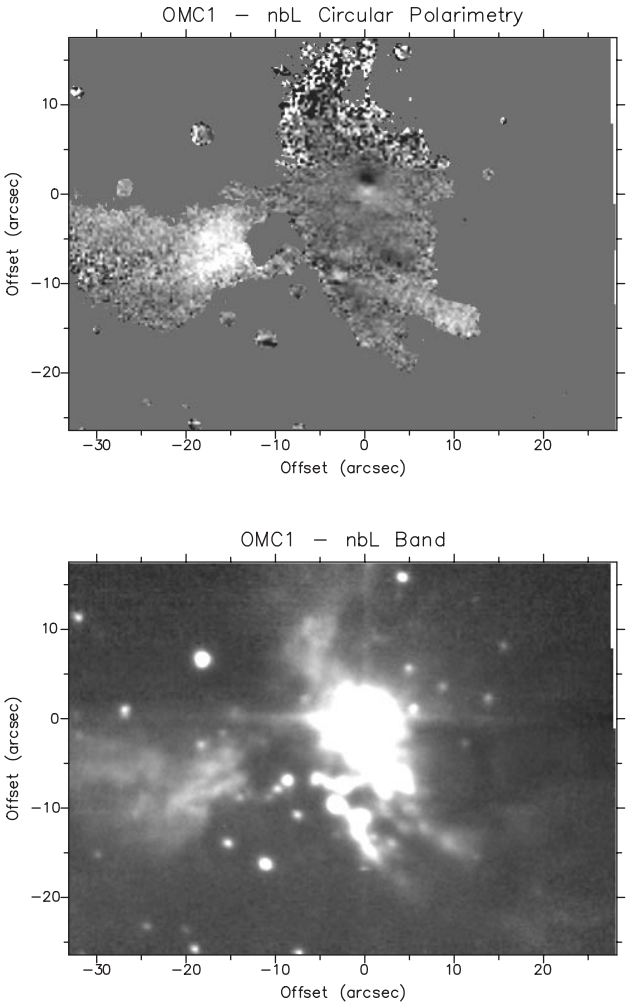


**Figure 6.** Narrow $L$-band (nb$L$) imaging circular polarimetry of the OMC-1 region. The top panel shows the polarimetry scaled between −1 per cent (black) and +5 per cent (white). The observations have had low signal-to-noise ratio data masked out. The bottom panel shows the corresponding intensity distribution. Offsets are west from the BN object.

BN within a 10-arcsec aperture in the $K$ band to be $+1.56 \pm 0.18$ per cent. BN is saturated in our $K_n$-band images; however, our $H$-band measurement of $+2.52 \pm 0.05$ per cent in a 6-arcsec software aperture is consistent with this picture and with model predictions (Lee & Draine 1985).

Table 2 presents a summary of near-infrared polarimetry measurements for SEBN. The data are taken from Minchin et al. (1991) and from this work. We have chosen the SEBN region as it is a well-studied and documented region within OMC-1, and also has the highest degrees of circular polarization detected at all wavelengths studied in this work (apart from the $J$ band). This latter point probably indicates a very simple scattering geometry, thus simplifying any modelling. If the whole region were to be considered, the scattering geometry would be very complex owing to the many and varied physical processes occurring within the OMC-1 cloud and associated outflow.

Although the degrees of linear polarization of SEBN continue to increase with wavelength into the nb$L$ band, the circular polarization ceases to increase any further beyond the $K_n$ band. We note that the error on the nb$L$-band circular polarimetry is artificially higher than it should be. This is because, for SEBN, the

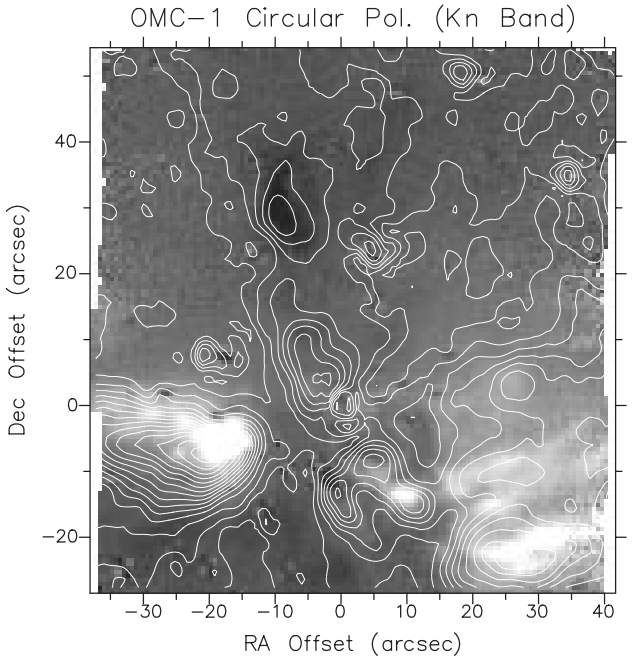


**Figure 7.** $K_n$-band circular polarimetry image from Fig. 1 overlaid with contours of the corresponding linear polarization as observed from the 1.3-m ISAS telescope in Japan (Geng 1993). Note the distinct correlation between high degrees of linear and circular polarization. A departure from this correlation is seen with the so-called 'red ridge' extending north-east from BN, as well as a small finger seen approximately 13 arcsec to the south of BN. These regions exhibit high linear polarization without a correspondingly high circular polarization component.

**Table 2.** Summary of polarimetry measurements (per cent) of SEBN.

| | *H* | *K* | nb*L* |
|---|---|---|---|
| Linear[a] | 14 ± 1.1 | 38 ± 1.2 | 57 ± 2.8 |
| Circular[b] | 6.2 ± 0.5 | 15.1 ± 0.3 | 9.4 ± 3.4 |
| Ellipticity | 0.44 ± 0.05 | 0.40 ± 0.01 | 0.16 ± 0.06 |

[a] From Minchin et al. (1991), measured within a 3 × 3 arcsec$^2$ aperture.
[b] Measured within a 3 × 3 arcsec$^2$ aperture.

nb*L*-band polarimetry becomes clumpy, increasing the scatter of the *V* Stokes parameter within the 3 × 3 arcsec$^2$ software aperture. The increased clumpiness of SEBN at this wavelength is probably a result of the increased spatial resolution of IRCAM3 over IRIS, combined with the fact that longer wavelength scattered radiation is more sensitive to dense clumps than at shorter wavelengths.

The ellipticity, expressed as the ratio of circular to linear polarization, is also calculated. This parameter is important as it is independent of any contaminating dilution effects that may be present as unpolarized light in the passbands (e.g. from the foreground H II region or intense molecular or atomic line emission), which have the effect of decreasing the degree of polarization. This means that the ellipticity can be used with high confidence to constrain the scattering and polarization mechanisms. This is investigated in the following section of the paper.

**Table 3.** Grain materials, refractive indices and size ranges used in the modelling.

| Grain material | Refractive index |
|---|---|
| Silicate | 1.7–0.03*i* |
| Organic refractory | 2.1–0.1*i* |
| Amorphous carbon | 2.77–0.8*i* |
| **Grain sizes** | **Range** |
| Large | 0.1–1.0 μm |
| Small | 0.005–0.25 μm |
| Medium-1 | 0.05–0.6 μm |
| Medium-2 | 0.03–0.8 μm |

## 4 MODELLING

### 4.1 Brief description of the model

The model used here is that developed by Gledhill & McCall (in preparation), in which they investigate the scattering of light off elongated and aligned grains. The basic input parameters of the model are the axial ratio (*a*/*b*), the Stokes vector of the incoming radiation (to cater for scattering both polarized and unpolarized radiation), its wavelength, the minimum and maximum grain sizes of a distribution [defined by a power-law index $\beta$, where $n(a) \propto a^{-\beta}$], the refractive index of the grain material and the direction of grain alignment relative to the scattering plane. It is implicitly assumed in this model that the alignment efficiency is 100 per cent (i.e. the grains are perfectly aligned).

The results are calculated by averaging the four Stokes intensities over a range of scattering angles, from 68° through to 112°. This range of angles was determined by measuring the angluar extent that SEBN subtends in Fig. 1 *as viewed from the position of IRc2* and assuming that it approximates a symmetrical volume in or near the same plane in the sky as IRc2.

Table 3 shows the size distributions and materials considered in our modelling. The grain compositions were chosen from Lucas & Roche (1998) and Li & Greenberg (1997) and were assumed to be wavelength-independent. In fact, there is a relatively small wavelength dependence (Li & Greenberg 1997) but this was ignored as it made little impact on our results and did not affect our conclusions.

### 4.2 The magnetic field and grain alignment directions

The magnetic field towards OMC-1 has recently been measured at millimetre, submillimetre and infrared wavelengths (Chrysostomou et al. 1994; Aitken et al. 1997; Rao et al. 1998; Schleuning 1998). The mid-infrared and millimetre studies of Aitken et al. and Rao et al. were not extensive enough to cover the SEBN region. The submillimetre and near-infrared work of Schleuning and Chrysostomou et al. covered a larger area in OMC-1 and implies that the field direction is of the order of 120°. We take this as the value of the magnetic field direction at the position of SEBN.

Fig. 8 provides a graphical description of the scattering geometry defined in the model. The grain can be aligned by applying two right-handed rotation transformations to it: one defined to be about the *Z*-axis (in the scattering plane) and the other about the *y*-axis (in the symmetry plane of the grains). To align the grain to 120°, these two rotations are given by $\phi = 90°$

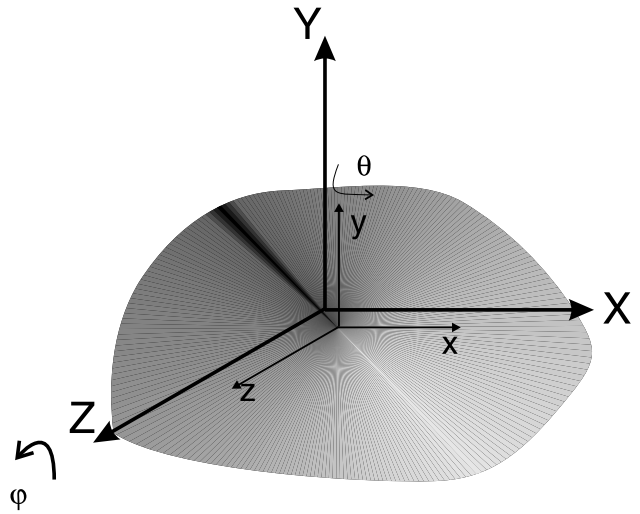


**Figure 8.** Schematic representation of coordinate axes used in the scattering model. *XYZ* represents the coordinate system for the photon, where the *XZ*-plane (shaded region) is the scattering plane. The coordinate system of the grain is given by *xyz*, where *z* is the symmetry axis of the grain. This grain can be aligned at any angle relative to the scattering plane by its right-hand rotation about the *Z*- and *y*-axes, given by $\phi$ and $\theta$, respectively.

and $\theta = 120°$. A crucial assumption which is made to simplify the calculations is that the scattering plane does not change relative to the symmetry axis of the grain.

### 4.3 Model results

#### *4.3.1 Scattering off aligned grains*

Silicates must form a component of the grain composition owing to their direct spectroscopic detection in OMC-1 (Aitken et al. 1985). The polarization spectrum of the silicate 9.7-μm absorption feature, obtained by Aitken et al., was modelled by Lee & Draine (1985) and Hildebrand & Dragovan (1995), who also studied similar silicate data of AFGL 2591 (Aitken et al. 1988), in an attempt to determine the shape of the absorbing material. Both authors promote oblate ($a/b < 1$) rather than prolate ($a/b > 1$) grains, albeit with some disagreement on the axial ratio – Lee & Draine favouring a value of $a/b \sim 0.5$ while Hildebrand & Dragovan prefer $\sim 2/3$. We note that this work is based on observations along the line of sight to BN, i.e. it is an 'average' of the material local to BN and through the OMC-1 cloud. Our observations of the SEBN region represent a localized region in the cloud (although the scattered radiation still needs to pass through the OMC-1 cloud), and there is no reason to believe that the grain shape will remain constant across the cloud. We ran models for both values of *a*/*b* for all grain materials and size distributions given in Table 3. In all cases, better results were obtained with an axial ratio of 0.5, and these are presented here.

Fig. 9 shows ellipticity results of scattering unpolarized radiation off aligned silicate grains. A range of indices between $\beta = 2$ and 5 were used for the power law describing the grain size distribution. Modelling the ellipticity in this way, although powerful, is not sufficient as the degrees of linear and circular polarization must also be satisfied. This means that the model polarization must be equal to or greater than the observed values, as dilution by unpolarized light can only decrease the polarization.

Organic refractory grains produced better results than amorphous carbon grains – the wavelength dependence of the ellipticity being too flat for the latter material. Fig. 10 shows results for the large and medium-2 populations for organic refractory grains.

The results indicate that larger grain models provide better fits to the data than small grain models, which completely fail to match the data. This suggests that the grains in the OMC-1 molecular cloud are significantly larger than are typically found in the interstellar medium (Rouan & Léger 1984). Furthermore, the results show that a largely absorptive grain material, such as carbon, is ruled out.

At this point, it is important to stress that the results shown in Figs 9 and 10 represent the upper limit where the grain alignment efficiency in the scattering cloud is 100 per cent. The alignment efficiency is probably much less than this – Hildebrand & Dragovan (1995) have estimated the Rayleigh reduction factor (the parameter describing grain alignment efficiency), in the line of sight to the BN object, to be ~0.25. In a model where aligned and randomly oriented grains co-exist, a number of photons will scatter from the randomly aligned population that will not carry any net circular polarization, but which will still be similarly linearly polarized to those photons scattered from the aligned grain population (Gledhill & McCall, in preparation). This has the net effect of diluting the circular polarization relative to the linear and thus decreasing the ellipticity.

The consequence to our model results is that the curves in Figs 9 and 10 will slide downward such that the best fits to the data will occur for models with $\beta \sim 3$.

#### *4.3.2 Scattering off spherical grains*

Spherical particles can also be simulated by setting the axial ratio to unity. In this case, it is only possible to produce circular polarization by scattering already polarized radiation. Shafter & Jura (1980) discuss the efficiency for conversion of linear polarization to circular polarization and find that carbonaceous grains, with a significant absorptive component to the refractive index, have the highest effciency for linear-to-circular conversion. Nevertheless, the conversion efficiencies never approach values greater than 0.5 for the size distribution that Shafter & Jura considered.

Fig. 11 shows model results for scattering 50 per cent linearly polarized radiation. As predicted by the models of Shafter & Jura, silicate grains were not able to produce high enough circular polarization to satisfy the results. Thus only results for the more absorptive organic refractory and amorphous carbon grains are shown.

The closest matches to the data were provided by the similarly sized medium-1 and medium-2 distributions. An exercise to check whether the results were variant with input linear polarization was also conducted by scattering 30 per cent linearly polarized radiation. The results showed that the linear polarization is largely invariant whereas the circular polarization is very dependent on the incident polarization. Using the medium-1 grain distribution and amorphous carbon grains, the best-fitting model changed from a power-law index of $\beta = 5$ to $\beta = 3$.

However, the problem that this model faces compared with the aligned grains model is that the output linear polarizations (and the circular polarization to some extent) are very high. A large amount of dilution would be required to bring the degrees of linear polarization down to meet those observed. For instance, at 3.6 μm

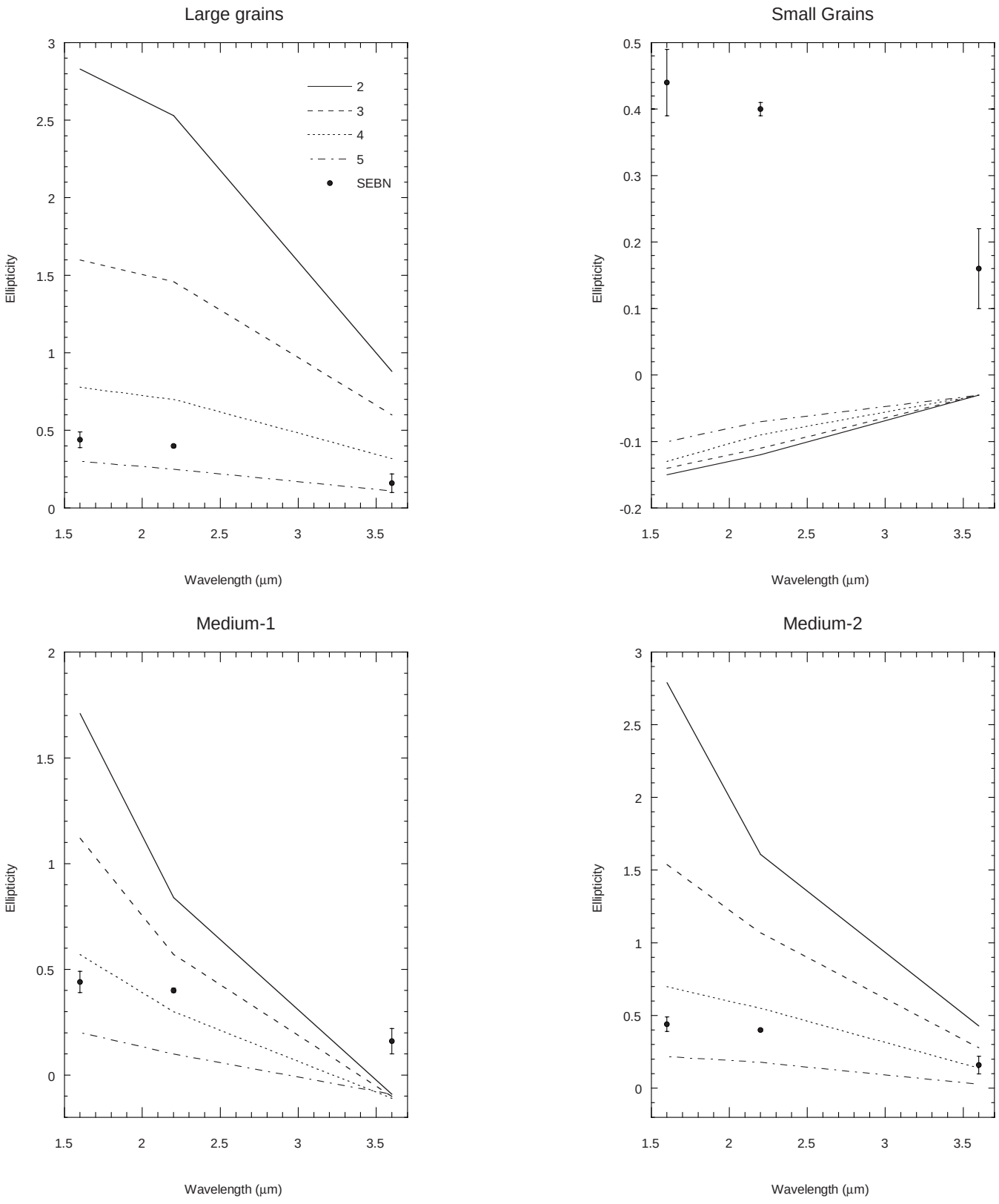


**Figure 9.** Model results of the ellipticity for scattering off aligned silicate grains. Results are shown, within each panel, for four size distributions described by the power-law index $\beta = 2$ (solid line), 3 (dashed line), 4 (dotted line) and 5 (dash–dotted line). Data points for the SEBN region of OMC-1 are also shown.

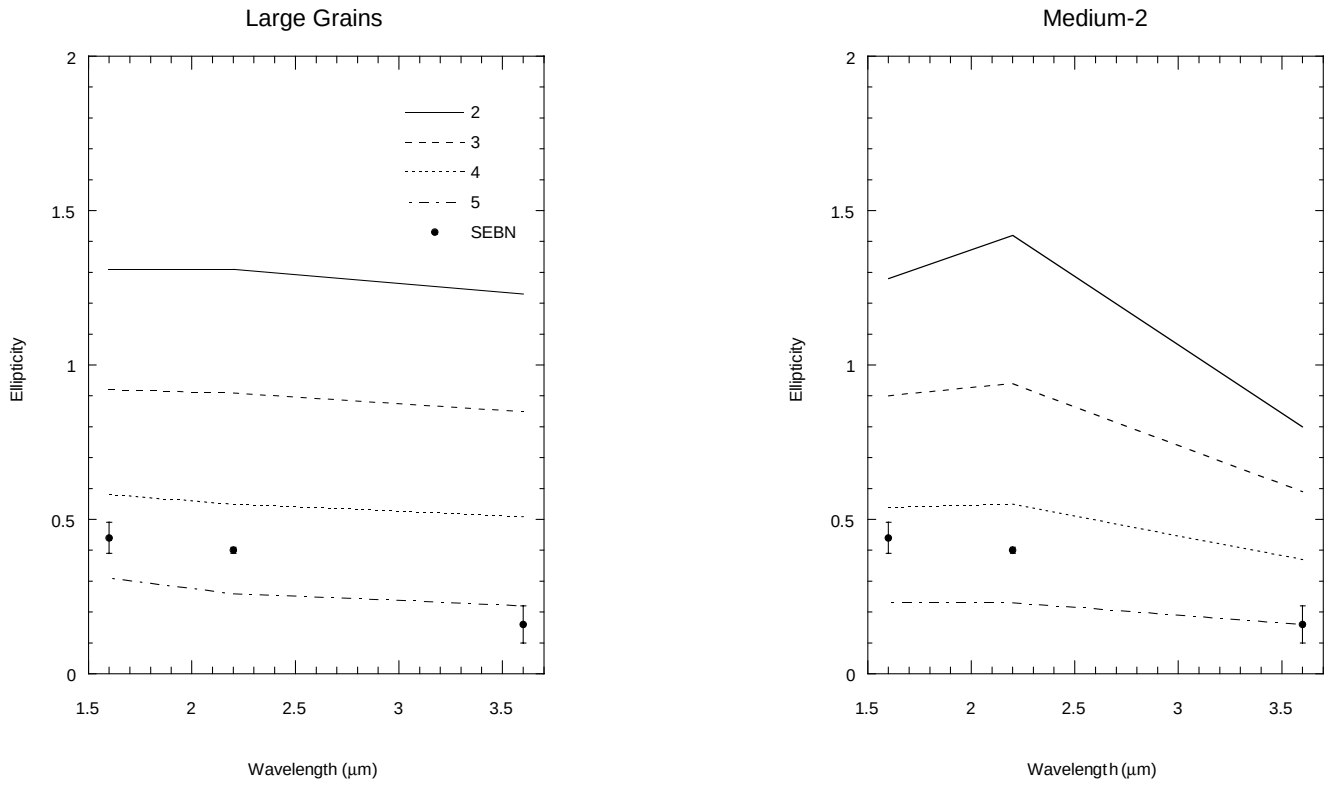


**Figure 10.** As Fig. 9 but for organic refractory grains. Only results for the large and medium-2 grain models show a satisfactory fit to the data, for distributions described by a power-law index between $\beta = 4$ and 5. Data points for the SEBN region of OMC-1 are also shown.

(where any dilution at the position towards SEBN would be at its minimum) the model linear polarization is typically 70–80 per cent. To get to 50 per cent linear polarization, we would require the polarized radiation to be diluted by 40–60 per cent. It is not clear where this amount of unpolarized radiation would originate. The SEBN area may be associated with a clump of very hot dust, but this is not evident from recent mid-infrared imaging of the BN/KL region which shows low colour temperatures associated with the SEBN area (Gezari et al. 1998).

It would be possible to solve this problem if a wider range of scattering angles were used. This could only occur, however, if the SEBN area were in fact elongated by a factor of 2 or more along the line of sight. Thus, as a caveat, we conclude that, while we find the aligned grain scattering model attractive, it is not certain at this stage that it represents the final solution to the immediate problem.

## 5 DISCUSSION

### 5.1 The cloud morphology

We now discuss the implications of these polarimetry (linear and circular) results for the morphology of the OMC-1 cloud. It has already been demonstrated that there are two aspects to the polarimetry from OMC-1 – regions with high polarization and regions with low polarization.

#### *5.1.1 Regions with low polarization*

Regions with relatively low degrees of polarization ($p_{\rm linear} \sim 5$ per cent and $p_{\rm circular} \sim 2$ per cent in the $K$ band) pervade the bulk of the OMC-1 region. The circular polarization exhibits a quadrupolar pattern of alternating sign centred about the vicinity of IRc2 and BN (see Fig. 2), a pattern which can be readily generated from polarized source and Monte Carlo models (Gledhill et al. 1996; Fischer et al. 1996; Chrysostomou et al. 1997a). Light from the central source is scattered a number of times (most probably in an accretion disc or disc envelope) before escaping into the outflow from where it is then scattered towards us.

The cavity walls of the outflow constitute hot material that has recently been disturbed by the passage of shocks which are clearly seen in $H_2$ images of OMC-1 (Allen & Burton 1993; Schild, Miller & Tennyson 1997; Stolovy et al. 1998). It is not expected that, in this environment, grains would retain any previous alignment that they may have had. Hence the scattering in the outflow regions will be off randomly oriented particles.

The fact that the linear polarization in the $K$ band is only $\sim$5 per cent is in support of this, as we expect to achieve much higher degrees of linear polarization from spherical particles (Mie scattering) at this wavelength (Clark & McCall 1997).

Put simply, we can understand the pervading pattern of linear and circular polarization in the context of a bipolar outflow and a polarized source, scattering radiation off randomly oriented grains.

**Figure 11.** Ellipticity models for scattering off spherical grains with an input polarization of 50 per cent. Only results for the medium-1 and medium-2 size distributions are shown, as they provide the closest fit to the data. The top graphs are for organic refractory grains, and the bottom ones are for amorphous carbon.

## Organic Refractory Grains

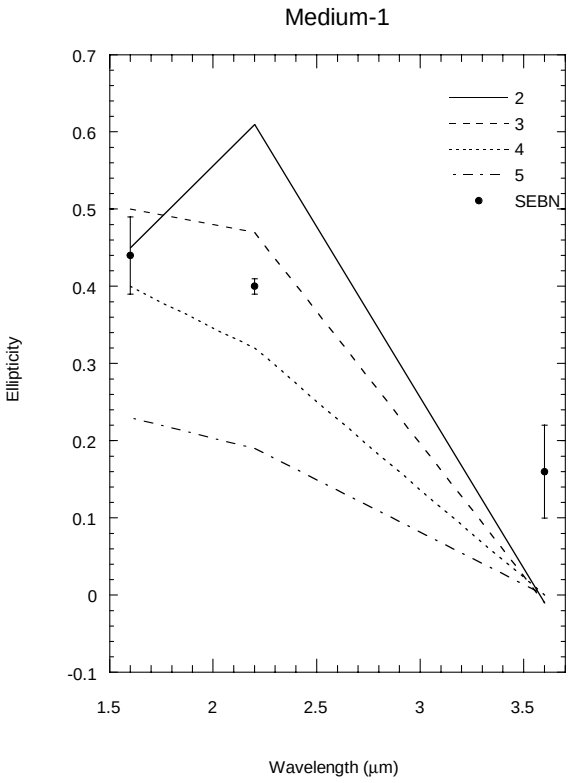


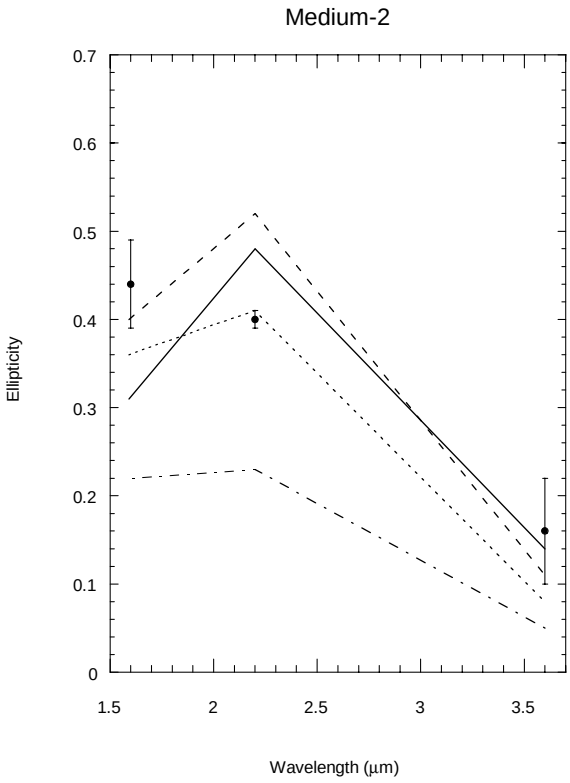


## Amorphous Carbon Grains

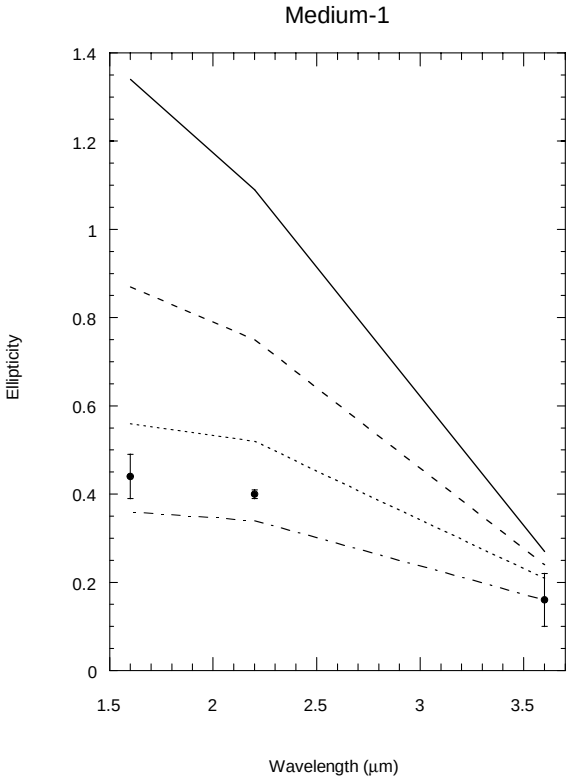


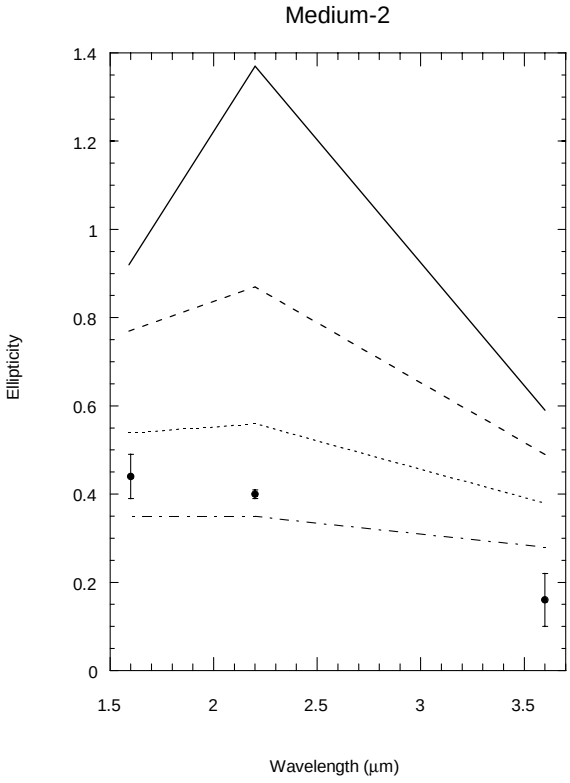

#### 5.1.2 *Regions with high polarization*

Regions with higher degrees of circular polarization are generally associated with high degrees of linear polarization in OMC-1 (see Fig. 7). Our modelling of the ellipticity of polarization suggests that the origin of this polarization is scattering off aligned grains. To reconcile this with our conclusions regarding regions with low polarization, we must have those regions with high polarization comprising material that is physically separate from the outflow, but nearby. Thus the grains would not have had their alignment disturbed by the outflow.

It is therefore necessary that these regions enjoy direct views of the illuminating source. Evidence in support of this has recently been provided in two independent studies (and we believe our data form a third).

(i) The first detection of the $H_2$ $v = 8$–6 O(5) line in Orion was recently reported (Schild et al. 1997, see their fig. 6), and showed it to be spatially coincident with SEBN. The excitation energy for this line is $\sim 40\,000$ K, a temperature at which $H_2$ would not normally survive. Thus its detection means that either the $H_2$ is excited by UV photons from an illuminating source that has a direct view of SEBN, or the $H_2$ $v = 8$–6 O(5) photons are formed much closer to the illuminating source and are then scattered to us off SEBN. Either way, a direct view of the IRc2 region by SEBN is required.

(ii) Morino et al (1998) detected 2-μm absorption features of CO $\Delta v = 2$ bandheads, as well as neutral Na I and Ca I, at the positon of SEBN, thus claiming that they had measured the *reflected* spectrum of the IRc2 region.

By direct implication from the arguments above, we also infer that the other regions of high linear and circular polarization also see a direct view of the illuminating source. Unfortunately, Morino et al. (1998) did not observe in other parts of the nebula, and the image of Schild et al. (1997) did not go deep enough to detect the weak $H_2$ $v = 8$–6 O(5) line in any other region apart from the immediate vicinity of BN. Since the excitation of this line is dependent on UV flux, the extinction to the more distant regions with high polarization may be too large.

At first sight, this morphological model may not be very appealing, and we should attempt to explain our observations in some other way. We have shown that the high degrees of circular and linear polarization must be due to scattering off aligned grains. The modelling of SEBN required the use of a narrow range of scattering angles. Scattering across the outflow region would occur over a relatively large range of scattering angles [owing to the large opening angle of the bipolar outflow cavities (Minchin et al. 1991)], thus serving to average the resultant degrees of polarization to lower values. However, if we still insist that the grains in the outflow (cavity walls) are not aligned, then this presents a problem as we know that scattering of polarized radiation off non-aligned spherical grains does not satisfy the SEBN measurements.

Taking this into consideration, it seems that the model requiring two separate scattering regions (scattering off randomly oriented grains in the outflow and off aligned grains in isolated regions around OMC-1) is the preferred one.

#### 5.1.3 *Relation to the Orion 'bullets'*

The spatial distribution of regions with high polarization is mainly to the south-west and south-east of the source. If these regions are exposed directly to the illuminating source, as we suggest, then there must be a physical mechanism operating that is able to open up such routes for the photons. We propose the Orion 'bullets' (Taylor et al. 1984; Allen & Burton 1993) as a possibility.

Recent dramatic images from NICMOS on the *Hubble Space Telescope* have shown that there is a cluster of bullets that are escaping from the core of OMC-1 (Stolovy et al. 1998; Schultz et al. 1999), which have the potential of having recently opened up gaps in the thick circumstellar material about IRc2.

### 5.2 Implications for the origins of life

The observations presented here have recently been used to help explain the chirality of organic molecules found on Earth and thus provide an insight into the origins of life (Bailey et al. 1998). The homochirality of biological molecules [the use of only left-handed (L-) amino acids and only right-handed (D-) sugars] has long been known to be an important characteristic of life, and yet its origins remain a mystery (Bonner 1991). The recent discovery of an excess of L-amino acids in the Murchison meteorite (Cronnin & Pizzarello 1997) has fuelled speculation that homochirality is extraterrestrial in origin.

One possible physical mechanism that can introduce an asymmetry in the chiral balance of molecular structures is UV photolysis by circularly polarized light. The asymmetry of the two chiral forms presents itself as an energy difference in the absorption bands. Circularly polarized light, since it has the same type of asymmetry as chiral molecules, can therefore distinguish between left- and right-handed molecules in its interactions. So, circularly polarized UV radiation can be selectively absorbed by one type of chiral molecule (circular dichroism) and thus destroy it – asymmetric photolysis (Shibata et al. 1998).

If, as described in Section 5.1, the regions with high circular polarization are directly viewing the illuminating source, then this provides an avenue by which UV light can escape the heavily embedded confines of the circumstellar disc. In fact, the detection of the $H_2$ $v = 8$–6 O(5) line by Schild et al. (1997) may be indicating that UV radiation is escaping at least as far as the SEBN region [$\sim$20 arcsec or 9000 au, assuming a distance of 450 pc to Orion (Genzel & Stutzki 1989)].

In conclusion, our discovery of high degrees of circular polarization in OMC-1 provides a plausible hypothesis which states that the chiral asymmetry of molecules is introduced in the pre-solar nebula and is then delivered to the surface of the planet during the 'heavy bombardment' phase after planet formation.

## 6 CONCLUSIONS

We have presented the first imaging circular polarimetry of OMC-1, measured in the $J$, $H$, $K_n$ and nb$L$ bands. The data show a complex polarization pattern, with high degrees of circular polarization present in isolated regions superimposed on to a quadrupolar pattern of low polarization ($\sim$1–2 per cent). To this date, our detection of 17 per cent circular polarization in the $K_n$ band is the highest circular polarization measured for any young stellar object.

The spatial correlation of high linear and circular polarization is demonstrated, indicating a common mechanism for the two. We separate the polarization structure into two distinct components – a high-polarization component and a low-polarization component.

(i) The low-polarization component pervades the whole region

with a circular polarization of the order of $\pm 2$ per cent in the $K_n$ band. It exhibits a quadrupolar pattern of alternating sign of circular polarization about the source IRc2. This pattern has been previously observed in other young stellar objects with outflows, and can be explained in the context of a polarized source model and scattering off non-aligned aspherical grains (i.e. multiple scattering).

(ii) We explain the regions of high polarization as scattering of unpolarized radiation off aligned, oblate grains. A model for scattering off aligned grains, developed by Gledhill & McCall (in preparation), is used to model the ellipticity of the polarization (the ratio of circular to linear polarization) from the bright and highly polarized SEBN region (Aitken et al. 1985). The results indicate that the grains are composed of silicate and/or organic refractory material, and that they need to be significantly larger than grains typically found in the interstellar medium.

To explain these components in OMC-1 self-consistently, we have put forward a morphological model which requires that the regions producing high polarization scatter radiation viewed directly from the central source and are separate, but near to, the main body of the outflow region. The high polarization is produced by the scattering of unpolarized radiation off elongated and aligned grains. Regions with low polarization are produced by the scattering occurring off (and within) the outflow cavities. The very low degrees of linear polarization measured in the outflow regions argue for randomly oriented ellipsoids for the scattering grains, as spherical particles would produce significantly higher degrees of linear polarization. This allows us to have the same grain properties throughout the OMC-1 cloud, with the grains in the outflow cavities having had their alignment destroyed by the passage of shocks, whereas those grains associated with high degrees of polarization have remained undisturbed.

The results presented here have significance for theories of the origins of life. The requirement that we have imposed on the cloud morphology – the presence of regions near to and with a direct view of the illuminating source – represents the ideal morphology required by Bailey et al. (1998) to explain how circularly polarized UV radiation can penetrate into a molecular cloud and thus directly influence the chiral symmetry of organic molecules in the parent cloud. This material then goes on to form stars, planets and (perhaps) life.

Our ability to obtain information on the source morphology and structure, as well as the physical parameters of the constituent grains, clearly demonstrates the diagnostic power available when linear *and* circular polarimetry is obtained with a broad wavelength baseline.

## ACKNOWLEDGMENTS

We thank the staff at the Anglo-Australian Telescope and the United Kingdom Infrared Telescope for their enthusiastic and continued support of polarimetry. The United Kingdom Infrared Telescope is operated by the Joint Astronomy Centre on behalf of the UK Particle Physics and Astronomy Research Council. We thank the Department of Physical Sciences, University of Hertfordshire, for providing polarimetric facilities for infrared instrumentation at both the AAT and UKIRT. FM acknowledges financial support from the France–Australia Collaboration, supported by the Ministry of National Education, Research and Technology of France. We also thank Dr Yukiyasu Kobayashi for providing us with a digital image of the linear polarization in OMC-1, shown in Fig. 7.

## REFERENCES

Aitken D. K., Bailey J. A., Roche P. F., Hough J. H., 1985, MNRAS, 215, 815
Aitken D. K., Roche P. F., Smith C. F., James S. D., Hough J. H., 1988, MNRAS, 230, 629
Aitken D. K., Smith C. H., Moore T. J. T., Roche P. F., Fujiyoshi T., Wright C. M., 1997, MNRAS, 286, 85
Allen D. A., Burton M. G., 1993, Nat, 363, 54
Bailey J. A., Chrysostomou A., Hough J. H., Gledhill T. M., McCall A., Clark S., Ménard F., Tamura M., 1998, Sci, 281, 672
Bonner W. A., 1991, Orig. Life, 21, 59
Chrysostomou A., Hough J. H., Burton M. G., Tamura M., 1994, MNRAS, 268, 325
Chrysostomou A., Ménard F., Gledhill T. M., Clark S., Hough J. H., McCall A., Tamura M., 1997a, MNRAS, 285, 750
Chrysostomou A., Burton M. G., Axon D. J., Brand P.W.J.L., Hough J. H., Bland-Hawthorn J., Geballe T. R., 1997b, MNRAS, 289, 605
Clark S. G., McCall A., 1997, MNRAS, 284, 513
Cronnin J. R., Pizzarello S., 1997, Sci, 275, 951
Fischer O., Henning Th., Yorke H. W., 1996, A&A, 308, 863
Geng F., 1993, PhD thesis, University of Tokyo
Genzel R., Stutzki J., 1989, ARA&A, 27, 41
Gezari D. Y., Backman D. E., Werner M. W., 1998, ApJ, 509, 283
Gledhill T. M., Chrysostomou A., Hough J. H., 1996, MNRAS, 282, 1418
Gonatas D. P. et al., 1990, ApJ, 357, 132
Hildebrand R. H., Dragovan M., 1995, ApJ, 450, 663
Hough J. H., Chrysostomou A., Messinger D. W., Whittet D. C. B., Aitken D. K., Roche P. F., 1996, ApJ, 461, 902
Lee H. M., Draine B. T., 1985, ApJ, 290, 211
Li A., Greenberg J. M., 1997, A&A, 323, 566
Lonsdale C. J., Dyck H. M., Capps R. W., Wolstencroft R. D., 1980, 238, L31
Lucas P. W., Roche P. F., 1998, MNRAS, 299, 699
Menten K. M., Reid M. J., 1995, ApJ, 445, L157
Minchin N. R. et al., 1991, MNRAS, 248, 715
Morino J.-I., Yamashita T., Hasegawa T., Nakano T., 1998, Nat, 393, 340
Rao R., Crutcher R. M., Plambeck R. L., Wright M. C. H., 1998, ApJ, 502, L75
Rouan D., Léger A., 1984, A&A, 132, L1
Schild H., Miller S., Tennyson J., 1997, A&A, 319, 1037
Schleuning D. A., 1998, ApJ, 492, 811
Schultz A. S. B., Colgan S. W. J., Erickson E. F., Kaufman M. J., Hollenbach D. J., O'Dell C. R., Young E. T., Chen H., 1999, ApJ, 511, 282
Shafter A., Jura M., 1980, AJ, 85, 1513
Shibata T., Yamamoto J., Yonekubo S., Osanai S., Soai K., 1998, J. Am. Chem. Soc., 120, 12157
Stolovy S. R. et al., 1998, ApJ, 492, L151
Taylor K. N. R., Storey J. W. V., Sandell G., Williams P. M., Zealey W. J., 1984, Nat, 311, 236
Werner M. W., Capps R. W., Dinnerstein H. L., 1983, ApJ, 265, L13

This paper has been typeset from a TEX/LATEX file prepared by the author.